RSC Advances

PAPER

View Article Online
View Journal | View Issue

Cite this: *RSC Adv.*, 2015, **5**, 103451

Significantly enhancing the stability of a Cu_2ZnSnS_4 aqueous/ethanol-based precursor solution and its application in $Cu_2ZnSn(S,Se)_4$ solar cells†

Zhen-Yu Xiao,[ab] Yong-Feng Li,*[ab] Bin Yao,*[ab] Zhan-Hui Ding,[b] Rui Deng,[c] Hai-Feng Zhao,[d] Li-Gong Zhang[d] and Zhen-Zhong Zhang[d]

Received 2nd November 2015
Accepted 16th November 2015

DOI: 10.1039/c5ra23015b

www.rsc.org/advances

The stability of a CZTS precursor solution plays an important role for potential industrial applications, and could provide insight into the understanding of the solubility mechanism of the raw materials. In this work, we report a systematic investigation on the stability of a metal/thiourea aqueous/ethanol-based precursor solution used for fabricating Cu_2ZnSnS_4 (CZTS) thin films. It is found that the metal/thiourea aqueous/ethanol solution is metastable, and easily produced a mass of precipitation when the solution was prepared for few hours. This could cause an element to be missed out of the film, giving a very bad film-processing ability, and effect the application of such a method. So we studied in detail the crystalline precipitation through SEM, EDS and FTIR, and found that they mainly contain copper ion and thiourea coordination complexes. Furthermore, we demonstrated that the low-toxicity 3-mercaptopropionic acid (MPA) can play an important role as an auxiliary ligand in the precursor solution. Addition of MPA into the precursor solution can avoid the precipitation and noticeably improve the stability of the precursor solution from ~3 hours to 1 week. Using the precursor solution with added MPA, we fabricated a single phase of a CZTS film, and prepared a large-grain and hole-free $Cu_2ZnSn(S,Se)_4$ (CZTSSe) film. More importantly, a CZTSSe film solar cell with a competitive power conversion efficiency of 7.25% has been reported in this work.

Introduction

Kesterite $Cu_2ZnSn(S,Se)_4$ (CZTSSe), as an alternative for $Cu(In,Ga)(S,Se)_2$ (CIGSSe) and CdTe, has attracted much attention over the past several years, due to its direct bandgap being close to the optimum bandgap of 1.0–1.5 eV, having a high absorption coefficient (>10^4 cm^{-1}) and containing earth-abundant as well as environmentally-friendly constituents.[1–3] Up to now, many efficient strategies have been used to fabricate CZTSSe absorber layers, such as thermal co-evaporation,[4–6] sputtering,[7–10] electrodeposition[11,12] and the solution approach,[13–20] *etc.* Among these deposition methods, the solution approach, as a form of non-vacuum-deposition technology, is considered as an excellent choice for obtaining smooth and high-quality CZTSSe absorber layers, and could offer the potential to significantly lower the manufacturing cost of solar cells compared to the vacuum-deposition technologies. The CZTSSe-based solar cell prepared by the hydrazine-based solution approach has demonstrated a record power conversion efficiency (PCE) of 12.6%.[20] However, since hydrazine is a highly toxic and explosive compound which must be handled in an inert environment such as an N_2-filled glove box, the hydrazine-based approach is difficult to use to prepare CZTSSe-based solar cells in practice. Therefore, it is necessary to develop a kind of non-harmful, low-cost and environmentally-friendly solution approach.

Aqueous/ethanol-based solution approaches are considered as green and low-cost preparation methods of CZTS due to them not containing highly toxic organic solvent. Some research groups have used this approach to prepare kesterite CZTS films.[21–23] Compared with other aqueous/ethanol-based solution approaches, the metal/thiourea aqueous/ethanol-based precursor solution approach is considered to be superior in simplifying fabrication processing, and reducing fabrication costs and environmental damage. Such a solution process was first reported by Li's group and demonstrated a conversion efficiency of 6.2% under AM 1.5G simulated sunlight.[23] However, we found that the metal/thiourea aqueous/ethanol-

[a]*Key Laboratory of Physics and Technology for Advanced Batteries (Ministry of Education), College of Physics, Jilin University, Changchun, 130012, China. E-mail: liyongfeng@jlu.edu.cn; binyao@jlu.edu.cn*

[b]*State Key Lab of Superhard Materials, College of Physics, Jilin University, Changchun 130012, China*

[c]*School of Materials Science and Engineering, Changchun University of Science and Technology, Changchun, 130022, China*

[d]*State Key Laboratory of Luminescence and Applications, Changchun Institute of Optics, Fine Mechanics and Physics, Chinese Academy of Sciences, No. 3888 Dongnanhu Road, Changchun 130033, PR China*

† Electronic supplementary information (ESI) available: EDS patterns of the as-fabricated and selenized CZTS-A(B) films. See DOI: 10.1039/c5ra23015b

based precursor solution approach is metastable and precipitation occurs soon after preparation due to the high concentrations of metal salts and thiourea, leading to an unstable solution.[24] Such a metastable solution is hard to use to fabricate a single-phase kesterite CZTS thin film and limits the potential applications. Therefore, it is necessary to understand the mechanism and develop a simple route which could noticeably improve the stability of the metal/thiourea aqueous/ethanol-based solution, and hence fabricate CZTS-based solar cells with high PCEs.

In this work, we systematically investigated the stability of the metal/thiourea aqueous/ethanol-based precursor solution. The solution easily crystallizes, and then the composition of the precursor solution becomes undesirable. Furthermore, the film-processing ability will get worse and smooth and hole-free CZTS films can't be obtained. Additionally, we study in detail the crystalline precipitation by SEM, EDS and FTIR. Interestingly, we find that the non-harmful 3-mercaptopropionic acid (MPA) can obviously improve the stability of the precursor solution and fabricated high-quality CZTS films. By tuning the composition of the CZTSSe thin film with selenized processing, a power conversion efficiency of 7.25% has been achieved by this stable aqueous/ethanol-based solution approach, which is comparable to values reported using aqueous/ethanol-based true solution processes.

Experimental

CZTS aqueous/ethanol-based precursor solution preparation

The CZTS aqueous/ethanol-based precursor solution was prepared by dissolving $CuCl_2 \cdot 2H_2O$ (0.4219 g, 2.475 mmol), $ZnCl_2$ (0.2453 g, 1.8 mmol), $SnCl_2 \cdot 2H_2O$ (0.3385 g, 1.5 mmol), and thiourea (0.9134 g, 12 mmol) into a mixture solution containing water (4 mL) and ethanol (2 mL) at room temperature. After stirring for 20 min, a clear CZTS aqueous/ethanol-based precursor solution was obtained.

Precipitation of the CZTS aqueous/ethanol-based precursor solution

When the CZTS aqueous/ethanol-based precursor solution was stored for three hours, some crystalline precipitates were observed clearly. In order to understand the mechanism affecting the stability of the precursor solution, the precipitates were collected by the centrifuging method, then were cleaned by deionized water and ethanol three times, and finally were dried at 60 °C for twelve hours.

Stable CZTS aqueous/ethanol-based precursor solution preparation

0.5 mL 3-mercaptopropionic acid (MPA) was added into the CZTS aqueous/ethanol-based precursor solution. After stirring the solution for a few minutes, a light yellow clean solution formed, and it could be stably stored in air for a week.

Preparation and selenization of the CZTS precursor thin film

Two kinds of CZTS thin films fabricated from the different types of CZTS precursor solutions were denoted as CZTS-A and CZTS-B, respectively. The as-prepared CZTS thin films were deposited on Mo-coated soda-lime glass (SLG) substrates by spin-coating the CZTS precursor solutions without and with MPA at 3000 rpm for 30 s, respectively, and then were annealed in air at 300 °C for 5 minutes. The coating and drying processes were repeated several times to obtain ~1.5 μm-thick films. The two films were selenized by loading them in a graphite box with a hole of 1 mm diameter together with some Se powders, then transporting into a rapid thermal processing furnace, and finally annealing for 20 minutes in the furnace which was heated to 540 °C at a heating rate of 5 °C s^{-1} with a nitrogen gas flow at normal pressure. After annealing, the films were subjected to cooling to room temperature naturally.

Device fabrication

The devices were prepared as a traditional CZTSSe-based solar cell structure, *i.e.* SLG/Mo/CZTSSe/CdS/i-ZnO/ITO/Al. Firstly, a CdS buffer layer (~50 nm) was deposited on the CZTSSe film by chemical bath deposition. Then, i-ZnO (~70 nm) and ITO (~250 nm) were sputtered on the top of the CdS layer followed by thermal evaporation of the Al grid electrode (~2 μm) on the top of the ITO layer. The details can be found elsewhere.[25] Finally, the whole device was mechanically scribed into 4 small cells with an active area of about 0.37 cm^2.

Characterization

The crystal structures of the CZTS and CZTSSe films were characterized by X-ray diffraction (XRD) with Cu Kα radiation ($\lambda = 1.5406$ Å). Raman spectra with an excitation wavelength of 532 nm were recorded using a Renishaw system. The scanning electron microscopy (SEM) measurement was performed using an Hitachi S-4800 equipped with an energy dispersive X-ray spectroscopy (EDS) system (EDAX Genesis 2000). The Fourier-transform infrared (FTIR) spectrum of the precipitate was measured using a Nicolet AVATAR 360 FTIR system. The PCE of the CZTSSe-based solar cells was determined by measurement of its current density–voltage curves under simulated AM 1.5G solar illumination, as calibrated with an official certified crystalline Si reference cell. The external quantum efficiency (EQE) was measured by a Zolix SCS 100 QE system.

Results and discussion

The stability of the CZTS precursor solution and the CZTS thin film fabrication process

Fig. 1 shows the flow diagram of the CZTS thin film fabrication process using the two kinds of CZTS aqueous/ethanol-based precursor solution. It indicates that some precipitates can be clearly observed at the bottom of the precursor solution without MPA when the solution is stored in air for 3 hours, and the CZTS thin film prepared by the solution without MPA has some big cavities with a diameter of ~2 μm, as shown in Fig. 1. However, for the CZTS precursor solution with MPA, no precipitate is

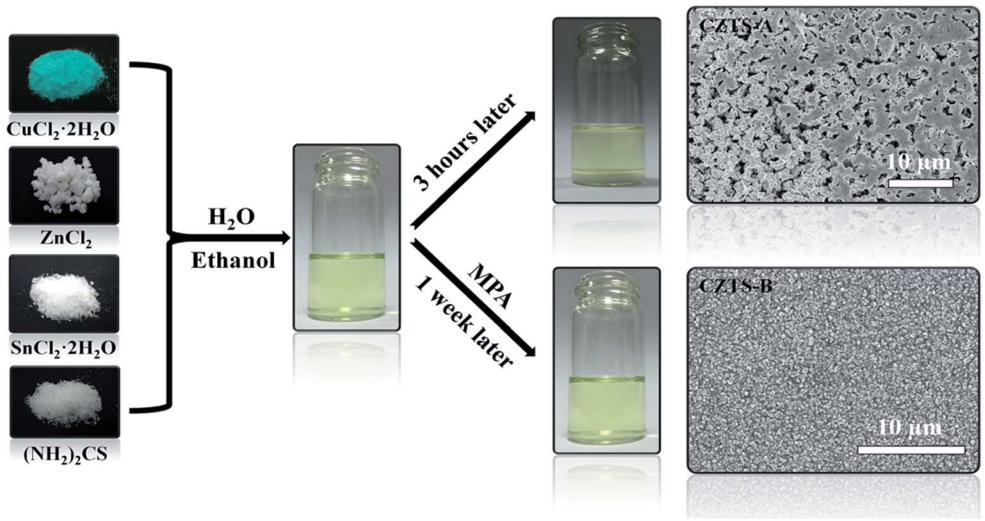

Fig. 1 Flow diagram of two kinds of CZTS thin film fabrication process. The right SEM images show the surface morphologies of the films (CZTS-A and CZTS-B) fabricated using the aqueous/ethanol-based precursor solution without and with MPA.

observed in it even though the solution is put in air for one week, revealing a good stability in air. In the previous reported works, thioglycolic acid showed a strong coordinating ability with Cu^{+}, Zn^{2+} and Sn^{4+}. We speculate that MPA plays a parallel role from the similar structures of MPA and thioglycolic acid. Furthermore, the CZTS thin film obtained using the solution with MPA (CZTS-B) shows it to be compact and hole-free, as shown in the SEM image in Fig. 1. The SEM results indicate that CZTS-B has a better crystal quality than CZTS-A, and hence can be used to fabricate high-efficiency CZTS-based solar cells compared to the CZTS-A thin film. The above results indicate that the addition of MPA not only can obviously improve the stability of the CZTS precursor solution, but also can enhance the crystal quality of the CZTS thin films due to the homogeneous composition.

Characterization of the precipitate and its effect on film quality

For investigating the morphology and composition of the precipitate, we analysed the precipitate using SEM, EDS and FTIR in detail. Fig. 2a shows the EDS spectrum of the precipitate. The SEM image and the composition of the precipitate are shown in the insets of Fig. 2a. The results of Fig. 2 indicate that the elements in the precipitate are N, C, S, Cu and Cl. Among these elements, C, N and S come from thiourea, while Cu and Cl come from $CuCl_2$. To confirm the chemical composition of the precipitate, FTIR measurement was performed, as shown in Fig. 2b. In the previous reported work, Hillhouse's group demonstrated that Cu^{2+} and Sn^{2+} could produce the oxidation–reduction reaction and then form Cu^{+} and Sn^{4+}. The FTIR absorbance bands at 3463, 3263 and 3162 cm^{-1} correspond to $-NH_2$ functional groups, and the 1604 cm^{-1} band is attributed to Cu(I) complexes and also attributed to NH_2 deformation.[26] The peaks at 1388 and 563 cm^{-1} are due to asymmetric N–C–N stretching and N–C–N bending vibrational modes in the molecule, respectively. Two peaks at 1095 and 709 cm^{-1} are attributed to C=S stretching.[26] Based on the EDX and FTIR results, it is concluded that the precipitate is composed of a Cu^{+}

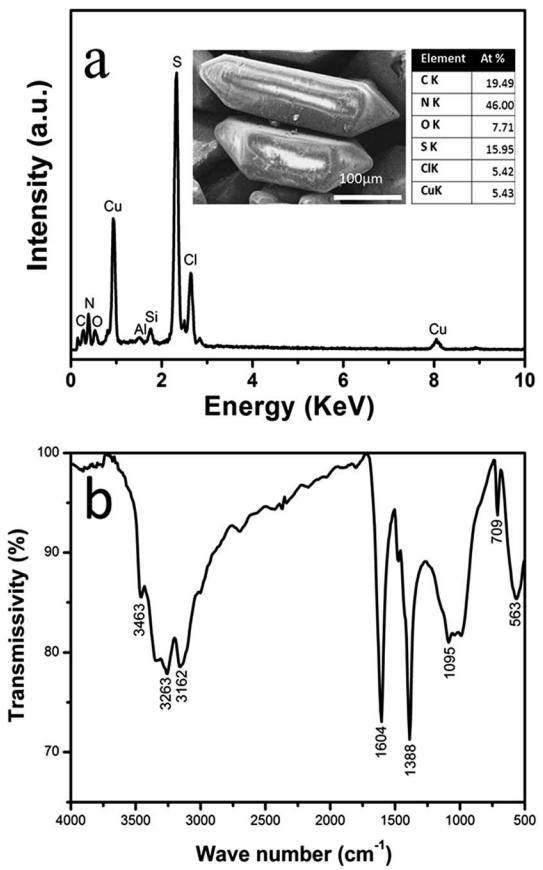

Fig. 2 EDS (a) and FTIR (b) spectra of the precipitate from the CZTS precursor solution without MPA. The inset shows the SEM image and the components of the precipitate.

and thiourea coordination compound. These results indicate that the coordination compound of Cu^+ and thiourea solution is easy to crystallize. Therefore, we proposed that the crystallizing mechanism of the copper salt and thiourea in the aqueous/ethanol solution formed coordination complexes (R = H_2O or ethanol) through the following reactions:

$$2Cu^{2+} + Sn^{2+} \rightarrow 2Cu^{+} + Sn^{4+} \quad (1)$$

$$Cu^{+} + Cl^{-} + x(NH_2)_2CS + yR \rightarrow Cu(Cl^{-})[(NH_2)_2CS]xRy\downarrow \quad (2)$$

The precipitation of Cu from the precursor solution without MPA will cause a serious lack of Cu in the CZTS-A film, as shown in Fig. S1 of the ESI,† which indicates that the Cu content in the CZTS-A and selenized CZTS-A is only about 7.24 and 4.36 at%, respectively, which is much smaller than the Cu content in stoichiometric kesterite CZTS and CZTSSe. To check the structures of the as-fabricated and selenized CZTS-A films, XRD and Raman spectra measurements were performed for the two films. Fig. 3(a) and (b) show the XRD pattern and Raman spectrum of the as-fabricated CZTS-A film, respectively, which indicate that the film is not composed of a single phase. Besides the kesterite CZTS phase, there also are SnS_2 and ZnS phases in the film,[27–31] and the CZTS and SnS_2 phases are dominant. Fig. 3(c) and (d) show the XRD pattern and Raman spectrum of the selenized CZTS-A film, respectively, which indicate that the film consists of kesterite CZTSSe, $Sn(S,Se)_2$ and Zn(S,Se) phases,[27–31] however, the $Sn(S,Se)_2$ phase is dominant. The results of Fig. 3 demonstrate that a single kesterite phase of CZTS or CZTSSe films cannot be fabricated using the unstable CZTS aqueous/ethanol-based precursor solution.

In order to avoid the precipitation and improve the stability of the CZTS aqueous/ethanol-based precursor solution, we added MPA into the aqueous/ethanol-based precursor solution. It was found that the precipitate dissolved completely, and moreover, that no additional precipitate was observed after one week, indicating that a stable CZTS aqueous/ethanol-based precursor solution was obtained.

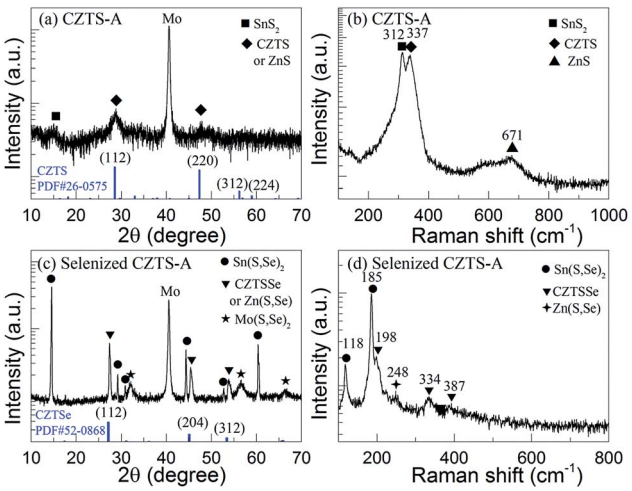

Fig. 3 XRD patterns and Raman spectra for the CZTS-A (a and b) and the selenized CZTS-A (c and d) thin films. The reference diffraction data of CZTS and CZTSSe are also presented at the bottom of (a) and (c), respectively.

Characterization of the CZTS and CZTSSe thin films

With the stable aqueous/ethanol-based precursor solution, a CZTS film (CZTS-B) was fabricated by spin-coating, while a CZTSSe film was obtained by selenizing the CZTS-B film. The XRD patterns of the CZTS-B and CZTSSe thin films are shown in Fig. 4(a), where only the (112), (220), and (312) diffraction peaks of CZTS with a kesterite structure are observed, suggesting that the CZTS-B film consists of a single kesterite CZTS phase. These diffraction peaks are very broad, implying that the CZTS-B thin film is composed of small-sized grains.[27–31] However, for the CZTSSe film (selenized CZTS-B), only the XRD diffraction peaks of kesterite CZTSSe are observed in the XRD pattern of the CZTSSe film, as shown in Fig. 4(a), and the diffraction peaks become very sharp, indicating that the CZTSSe film consists of a single kesterite CZTSSe phase with large-sized grains, which is highly desirable for high-efficiency CZTSSe solar cells.[27–31] It is also found that the diffraction peaks of CZTSSe shift toward lower angles compared to those of CZTS-B, which is attributed to the expansion of the unit cell volume induced by the partial replacement of S with Se. In addition, some minor peaks, such

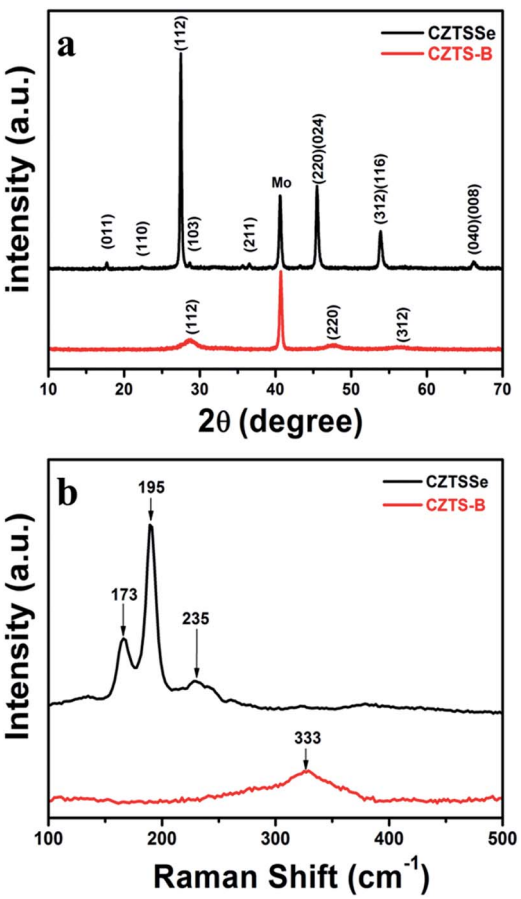

Fig. 4 XRD patterns (a) and Raman spectra (b) for the CZTS-B and the CZTSSe thin films (selenized CZTS-B).

as (011), (110), (103), (211), and (040)/(008), become observable, indicating that the CZTSSe thin film has good crystallinity.[27–31] The EDS measurements indicate that the chemical compositions of both films are closed to the stoichiometric ratio of CZTS and CZTSSe, as shown in Fig. S2 of the ESI.† The chemical composition of the CZTSSe film has a Cu/(Zn + Sn) ratio of 0.85 and a Zn/Sn ratio of 1.18, which are slightly different from those of the non-selenized CZTS thin film and are consistent with those reported previously for high-efficiency CZTSSe devices.[32,33]

It is well known that some binary and ternary sulfides and selenides, such as ZnS, ZnSe, Cu_2SnS_3, or Cu_2SnSe_3, have similar XRD patterns to kesterite CZTS or CZTSSe.[27–31] Therefore, XRD alone is insufficient to determine if there are other phases in the CZTS (or CZTSSe) thin films besides kesterite CZTS (or CZTSSe). Since Raman spectroscopy is able to identify the difference between CZT(S,Se) and the secondary phases, such as Cu_x(S,Se), Zn(S,Se), Sn(S,Se)$_2$, and Cu_2Sn(S,Se)$_3$, *etc.*, we examined the CZTS-B and CZTSSe thin films using Raman spectroscopy, as shown in Fig. 4(b). For the CZTS-B thin film, the major peak appears at 333 cm^{-1}, consistent with the literature reported previously,[28–30] indicating that a single phase of the kesterite CZTS thin film was obtained. For the CZTSSe thin film, the main peaks are located at 173, 195 and 235 cm^{-1}, which are in good agreement with the results of CZTSSe with S/(S + Se) ≈ 0.08 reported previously.[32] No Raman peak of the impurity phases, such as $Cu_x(S,Se)_y$, Zn(S,Se), Sn(S,Se)$_2$, and Cu_2Sn(S,Se)$_3$, are found in the Raman spectrum of the CZTSSe thin film, indicating that the CZTSSe film consists of a single phase of kesterite CZTSSe.[28–31]

The typical SEM images of the surface and cross-section of the CZTS-B thin film are shown in Fig. 5a and b, indicating that a uniform CZTS nanocrystalline thin film with a thickness of ~1.5 μm was formed by a consecutive spin-coating process. Fig. 5c shows the SEM image of the surface of the CZTSSe thin film, indicating that the surface is smoothing and its grain size is in the range between 1 and 3 μm. Moreover, most of the grain sizes are larger than 1.5 μm, which is desired for high-efficiency CZTSSe solar cells.[6,33,34] A cross-sectional SEM image of a completed CZTSSe solar cell is shown in Fig. 5d. The selenized CZTSSe thin film exhibits an obvious bi-layer morphology consisting of a dense large-grained top layer of about 1.1 μm and a fine-grain layer of about 400 nm near the Mo interface as well as a $MoSe_2$ layer of about 400 nm in thickness. A similar fine-grain layer has been observed by various groups for CZTSSe solar cells fabricated by the nanocrystal-based ink process and the molecular precursor solution approach.[34,35]

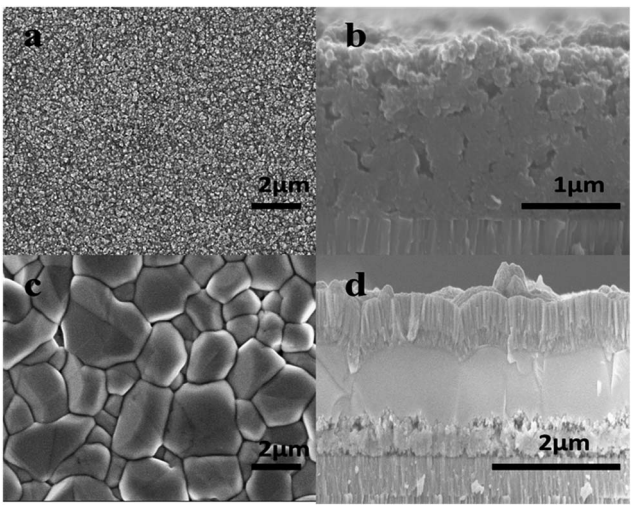

Fig. 5 Plane-view (a), and cross-sectional (b), SEM images of the as-fabricated CZTS thin film (CZTS-B). Plane-view (c), and cross-sectional (d), SEM images of the completed CZTSSe solar cell (selenized CZTS-B).

Characterization of device performance

The CZTSSe-based solar cell was fabricated with the conventional structure of SLG/Mo/CZTSSe/CdS/i-ZnO/ITO/Al. The current density–voltage (*J*–*V*) curves for a CZTSSe-based solar cell measured in the dark and under AM 1.5G illumination are shown in Fig. 6a. The as-fabricated device exhibits a PCE of 7.25% on the basis of an active area of 0.37 cm^2, an open circuit voltage of V_{oc} = 0.412 V, a short circuit current density of J_{sc} = 31.86 mA cm^{-2}, and a filling factor of FF = 55.2%. Fig. 6b shows the EQE spectrum of the CZTSSe-based solar cell, indicating that the highest quantum efficiency in the visible light range

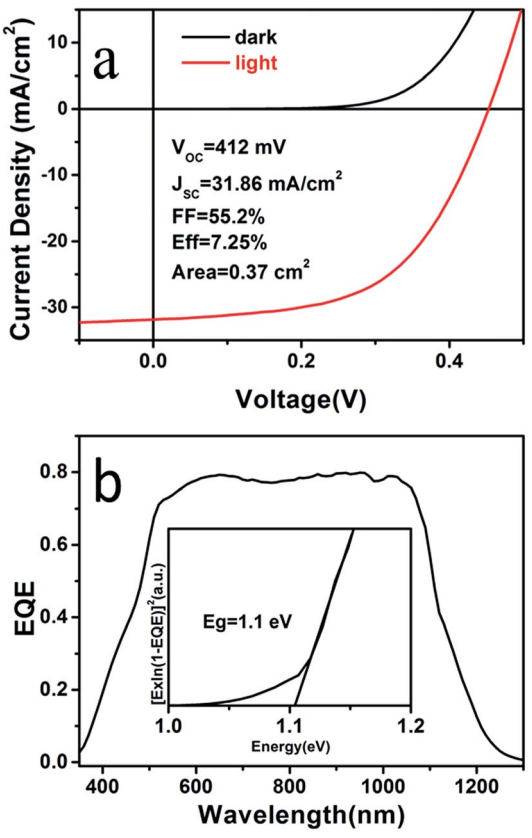

Fig. 6 (a) *J*–*V* curves of the CZTSSe thin film solar cell measured in the dark (black line) and under AM 1.5G illumination (red line). (b) EQE spectrum of the CZTSSe thin film solar cell. The inset in (b) shows the plot of $[E \times \ln(1 - \mathrm{EQE})]^2$ as a function of photon energy.

reaches ~80% in the wavelength range of 600–1050 nm. The bandgap of the CZTSSe absorber layer is calculated to be 1.1 eV, as shown in the inset of Fig. 6b. Compared to the record CZTSSe solar cells with a similar structure reported previously,[20] our PCE of 7.25% is smaller than that of the record CZTSSe (12.6%), which is mainly attributed to our V_{oc}, J_{sc}, FF and EQE values being much lower than those of the record CZTSSe solar cell ($V_{oc} = 0.513$ V, $J_{sc} = 35.2$ mA cm^{-2}, FF = 69.8% and EQE above 90%). The low J_{sc} and FF is due to the high serial resistance of our cell (1.03 Ω cm^2) being much higher than that of the record cell (0.2 Ω cm^2), while the V_{oc} and shunt resistance of our cell ($G = 0.8$ mS cm^{-2}) are low. It is well known that the serial resistance is related to the bulk resistance of the layers in the solar cell, such as the CZTS absorber, and CdS layers *etc.*, and the contact resistance of the electrodes, while the shunt resistance is related to the leakage current of the p–n joint. The serial resistance can be decreased by improving the crystal quality of these layers, and the decrease in the contact resistance and increase in the shunt resistance can be realized by optimizing the manufacturing techniques of the contact electrode and the p–n joint. As we know, the EQE is related to the structure of the solar cell, including an anti-reflection layer, the thickness and crystal quality of the emitting and absorbing layers and the recombination rate at the former and back surfaces. Compared to the structure of the record CZTSSe solar cell, our solar cell lacks an anti-reflection layer.[20] So, the low EQE may be due to there being no anti-reflection layer in our solar cell structure. Based on the above discussion, it can be expected that the PCE of the solar cell prepared by the aqueous/ethanol-based approach can be further enhanced by increasing the crystal quality of the layers, optimizing the structure of the solar cell and the preparation technologies of the contact electrodes and the p–n joint, and depositing an MgF_2 anti-reflection film.[36] Therefore, we believe that the aqueous/ethanol-based approach can become a promising preparation method of CZTS-based solar cells being low-cost and environmentally-friendly, though the PCE in the present work is still low compared to the record PCE.

Conclusions

In summary, we systematically studied the stability of the CZTS aqueous/ethanol-based precursor solution, and found that the precursor solution is metastable and precipitation occurs easily when it is stored for some hours. The precipitate is identified to contain a large amount of Cu^+ ions, which leads to the solution missing a large amount of Cu, and hence it cannot be used for the preparation of a single phase of kesterite CZTS. However, addition of non-harmful MPA into the precursor solution can avoid the precipitation and obviously improve the stability of the precursor solution. By adding MPA into the precursor solution, we fabricated a single phase of the CZTS film, and then obtained a large-grain and hole-free CZTSSe film by selenizing the as-prepared CZTS film. A CZTSSe thin film solar cell with a competitive power conversion efficiency of 7.25% has been achieved, which is obviously higher than that from the previously reported metal/thiourea aqueous/ethanol-based solution approach.

Acknowledgements

This work is supported by the National Natural Science Foundation of China under grant no. 10874178, 11074093, 61205038 and 11274135, the Specialized Research Fund for the Doctoral Program of Higher Education under grant no. 20130061130011, the Ph.D. Programs Foundation of Ministry of Education of China under grant no. 20120061120011, the Natural Science Foundation of Jilin province under grant no. 201115013, and the National Found for Fostering Talents of Basic Science under grant no. J1103202. The authors would like to thank Dr Gang Wang of Changchun Institute of Applied Chemistry for his helpful discussion and assistance with device fabrication.

Notes and references

1 D. B. Mitzi, O. Gunawan, T. K. Todorov, K. Wang and S. Guha, *Sol. Energy Mater. Sol. Cells*, 2011, **95**, 1421–1436.
2 K. Ramasamy, M. A. Malik and P. O'Brien, *Chem. Commun.*, 2012, **48**, 5703–5714.
3 H. Katagiri, K. Jimbo, W. S. Maw, K. Oishi, M. Yamazaki, H. Araki and A. Takeuchi, *Thin Solid Films*, 2009, **517**, 2455–2460.
4 B. Shin, O. Gunawan, Y. Zhu, N. A. Bojarczuk, S. J. Chey and S. Guha, *Progress in Photovoltaics: Research and Applications*, 2013, **21**, 72–76.
5 X. Yin, T. J. Huang, C. Tang, M. Du, L. Sun, Z. Shen and H. Gong, *Sol. Energy Mater. Sol. Cells*, 2015, **134**, 389–394.
6 Y. S. Lee, T. Gershon, O. Gunawan, T. K. Todorov, T. Gokmen, Y. Virgus and S. Guha, *Adv. Energy Mater.*, 2015, **5**, 1401372.
7 D. Zi-Yuan, L. Yong-Feng, Y. Bin, D. Zhan-Hui, Y. Gang, D. Rui, F. Xuan, W. Zhi-Peng and L. Lei, *J. Phys. D: Appl. Phys.*, 2014, **47**, 075304.
8 G. Yang, Y.-F. Li, B. Yao, Z.-H. Ding, R. Deng, J.-M. Qin, F. Fang, X. Fang, Z.-P. Wei and L. Liu, *J. Alloys Compd.*, 2015, **628**, 293–297.
9 J. J. Scragg, T. Ericson, X. Fontané, V. Izquierdo-Roca, A. Pérez-Rodríguez, T. Kubart, M. Edoff and C. Platzer-Björkman, *Progress in Photovoltaics: Research and Applications*, 2014, **22**, 10–17.
10 K. Moriya, K. Tanaka and H. Uchiki, *Jpn. J. Appl. Phys.*, 2007, **46**, 5780–5781.
11 H. Chen, Q. Ye, X. He, J. Ding, Y. Zhang, J. Han, J. Liu, C. Liao, J. Mei and W. Lau, *Green Chem.*, 2014, **16**, 3841.
12 F. Jiang, S. Ikeda, T. Harada, A. Ide, A. Mochihara, K. Yoshino and M. Matsumura, *RSC Adv.*, 2014, **4**, 24351.
13 H. Guo, Y. Cui, Q. Tian, S. Gao, G. Wang and D. Pan, *Cryst. Growth Des.*, 2015, **15**, 771–777.
14 C. Li, B. Yao, Y. Li, Z. Xiao, Z. Ding, H. Zhao, L. Zhang and Z. Zhang, *J. Alloys Compd.*, 2015, **643**, 152–158.
15 Z.-Y. Xiao, Y.-F. Li, B. Yao, R. Deng, Z.-H. Ding, T. Wu, G. Yang, C.-R. Li, Z.-Y. Dong, L. Liu, L.-G. Zhang and H.-F. Zhao, *J. Appl. Phys.*, 2013, **114**, 183506.

16 J. W. Cho, A. Ismail, S. J. Park, W. Kim, S. Yoon and B. K. Min, *ACS Appl. Mater. Interfaces*, 2013, **5**, 4162–4165.
17 H. Xin, J. K. Katahara, I. L. Braly and H. W. Hillhouse, *Adv. Energy Mater.*, 2014, **4**, 1301823.
18 G. Wang, W. Zhao, Y. Cui, Q. Tian, S. Gao, L. Huang and D. Pan, *ACS Appl. Mater. Interfaces*, 2013, **5**, 10042–10047.
19 Q. Tian, Y. Cui, G. Wang and D. Pan, *RSC Adv.*, 2015, **5**, 4184–4190.
20 W. Wang, M. T. Winkler, O. Gunawan, T. Gokmen, T. K. Todorov, Y. Zhu and D. B. Mitzi, *Adv. Energy Mater.*, 2014, **4**, 1301465.
21 M. Y. Yeh, C. C. Lee and D. S. Wuu, *J. Sol-Gel Sci. Technol.*, 2009, **52**, 65–68.
22 J. Zhong, Z. Xia, C. Zhang, B. Li, X. Liu, Y.-B. Cheng and J. Tang, *Chem. Mater.*, 2014, **26**, 3573–3578.
23 M. Jiang, F. Lan, X. Yan and G. Li, *Phys. Status Solidi RRL*, 2014, **8**, 223–227.
24 Y. E. Romanyuk, C. M. Fella, A. R. Uhl, M. Werner, A. N. Tiwari, T. Schnabel and E. Ahlswede, *Sol. Energy Mater. Sol. Cells*, 2013, **119**, 181–189.
25 G. Wang, S. Wang, Y. Cui and D. Pan, *Chem. Mater.*, 2012, **24**, 3993–3997.
26 S. Ariponnammal, S. Chandrasekaran and C. Sanjeeviraja, *Cryst. Res. Technol.*, 2012, **47**, 145–150.
27 D. Xia, Y. Zheng, P. Lei and X. Zhao, *Phys. Procedia*, 2013, **48**, 228–234.
28 J. J. Scragg, T. Ericson, X. Fontané, V. Izquierdo-Roca, A. Pérez-Rodríguez, T. Kubart, M. Edoff and C. Platzer-Björkman, *Progress in Photovoltaics: Research and Applications*, 2014, **22**, 10–17.
29 K. Wang, O. Gunawan, T. Todorov, B. Shin, S. J. Chey, N. A. Bojarczuk, D. Mitzi and S. Guha, *Appl. Phys. Lett.*, 2010, **97**, 143508.
30 L. Guo, Y. Zhu, O. Gunawan, T. Gokmen, V. R. Deline, S. Ahmed, L. T. Romankiw and H. Deligianni, *Progress in Photovoltaics: Research and Applications*, 2014, **22**, 58–68.
31 K. Wang, B. Shin, K. B. Reuter, T. Todorov, D. B. Mitzi and S. Guha, *Appl. Phys. Lett.*, 2011, **98**, 051912.
32 W. Yang, H.-S. Duan, B. Bob, H. Zhou, B. Lei, C.-H. Chung, S.-H. Li, W. W. Hou and Y. Yang, *Adv. Mater.*, 2012, **24**, 6323–6329.
33 J. Kim, H. Hiroi, T. K. Todorov, O. Gunawan, M. Kuwahara, T. Gokmen, D. Nair, M. Hopstaken, B. Shin, Y. S. Lee, W. Wang, H. Sugimoto and D. B. Mitzi, *Adv. Mater.*, 2014, **26**, 7427–7431.
34 Q. Guo, G. M. Ford, W.-C. Yang, C. J. Hages, H. W. Hillhouse and R. Agrawal, *Sol. Energy Mater. Sol. Cells*, 2012, **105**, 132–136.
35 Y. Cao, M. S. Denny, J. V. Caspar, W. E. Farneth, Q. Guo, A. S. Ionkin, L. K. Johnson, M. Lu, I. Malajovich, D. Radu, H. D. Rosenfeld, K. R. Choudhury and W. Wu, *J. Am. Chem. Soc.*, 2012, **134**, 15644–15647.
36 D. A. R. Barkhouse, O. Gunawan, T. Gokmen, T. K. Todorov and D. B. Mitzi, *Progress in Photovoltaics: Research and Applications*, 2012, **20**, 6–11.